Journal of Materials Chemistry A

PAPER

View Article Online
View Journal | View Issue

Cite this: J. Mater. Chem. A, 2019, 7, 15432

A Ca^{2+} MOF combining highly efficient sorption and capability for voltammetric determination of heavy metal ions in aqueous media†

Anastasia D. Pournara,[a] Antigoni Margariti,[b] Georgios D. Tarlas,[b] Andreas Kourtelaris,[c] Valeri Petkov,[d] Christos Kokkinos,[e] Anastasios Economou,[e] Giannis S. Papaefstathiou *[b] and Manolis J. Manos *[a]

We recently discovered that a Ca^{2+} two-dimensional framework, namely $[Ca(H_4L)(DMA)_2]\cdot 2DMA$ (**Ca-MOF**), was capable of exchanging the Ca^{2+} ions with Cu^{2+} almost quantitatively in a matter of seconds in aqueous solution. Herein, we report that **Ca-MOF** exhibits the capability of both removal and voltammetric determination of heavy metal ions in aqueous media. **Ca-MOF** shows one of the highest Pb^{2+} sorption capacities (~522 mg g^{-1}) reported for MOFs. More importantly, a column filled with **Ca-MOF** (1% wt) particles dispersed in silica sand (99% wt) can quantitatively remove traces of Pb^{2+} (~100 ppb) from a relatively large volume of a wastewater simulant solution (containing a large excess of competitive ions). **Ca-MOF** is also highly efficient for sorption of Cd^{2+}, Ni^{2+} and Zn^{2+}, even in the presence of several competitive cations. Actually, the Cd^{2+} sorption capacity (~220 mg g^{-1}) of **Ca-MOF** is one of the largest reported for MOFs. Furthermore, detailed Ni^{2+} and Zn^{2+} sorption studies of MOFs have not been described prior to this work. The mechanism of the M^{2+} (M^{2+} = Pb^{2+}, Cd^{2+}, Ni^{2+}, Zn^{2+}) exchange process was elucidated based on a series of spectroscopic, analytical and X-ray diffraction methods. In addition, a simple ready-to-use electrochemical sensor based on modified graphite paste with **Ca-MOF** was fabricated and successfully utilized for the determination of Pb^{2+}, Cd^{2+}, Cu^{2+} and Zn^{2+} at μg L^{-1} levels in aqueous solutions by anodic stripping voltammetry (ASV). Overall, this work demonstrates, for the first time, a dual function of a MOF as a sorbent and as an electrochemical sensor for heavy metal ions, thus opening a new window for materials with application in both environmental remediation and monitoring.

Received 28th March 2019
Accepted 28th May 2019

DOI: 10.1039/c9ta03337h

rsc.li/materials-a

Introduction

Heavy metal ions, such as Pb^{2+}, Cd^{2+}, Cu^{2+}, Ni^{2+}, Zn^{2+} *etc.*, represent the major contaminants for water resources. They are easily accumulated in the environment and living organisms and are highly toxic even at low concentrations (with the exception of Zn^{2+} which in low concentration is essential for humans and other species).[1] It is thus of vital importance to develop efficient and affordable methods for both the determination and the removal of these toxic species from water. Materials that can serve the dual function of sorption and detection-determination of heavy metal ions would be highly desirable; however, such materials are rare and are mainly limited to sorbents with the capability of luminescence sensing of heavy metal ions.[2]

Metal–Organic Frameworks (MOFs), which are crystalline polymeric metal complexes based on metal ions or clusters interconnected *via* polytopic organic ligands, have attracted great attention thanks to their unique structural features and potential applications in various fields.[3,4] MOFs combine a highly porous structure with tunable pore sizes and functionalities, thus being particularly promising for the sorption of pollutants. Several publications have described the use of MOFs as sorbents for ionic species. Among them, anion-exchange MOFs have been investigated in detail but MOFs with cation exchange properties are limited.[5]

Besides sorption, the detection of heavy metals is equally important. One of the most efficient, sensitive, and affordable

[a]Laboratory of Inorganic Chemistry, Department of Chemistry, University of Ioannina, 45110 Ioannina, Greece. E-mail: emanos@cc.uoi.gr

[b]Laboratory of Inorganic Chemistry, Department of Chemistry, National and Kapodistrian University of Athens, Panepistimiopolis, 157 71, Zografou, Greece. E-mail: gspapaef@chem.uoa.gr

[c]Department of Chemistry, University of Cyprus, 1678 Nicosia, Cyprus

[d]Department of Physics and Science of Advanced Materials Program, Central Michigan University, Mt. Pleasant, Michigan 48859, USA

[e]Laboratory of Analytical Chemistry, Department of Chemistry, National and Kapodistrian University of Athens, Panepistimiopolis, 157 71, Zografou, Greece

† Electronic supplementary information (ESI) available: EDS, PXRD, IR, NMR, TGA, PDFs and crystallographic data in CIF electronic format. CCDC 1905924 and 1905925. For ESI and crystallographic data in CIF or other electronic format see DOI: 10.1039/c9ta03337h

techniques that can be combined with simple and portable instrumentation for the determination of heavy metal ions is anodic stripping voltammetry (ASV).[6] Recently, there has been interest in the use of MOFs for such analytical purposes. Nevertheless, the development of MOF-modified electrodes for ASV of heavy metal ions is a challenging task and is still in its infancy.[7–11]

We recently described the synthesis and characterization of $[Ca(H_4L)(DMA)_2]\cdot 2DMA$ (**Ca-MOF**, Fig. 1), where H_6L is *N,N′*-bis(2,4-dicarboxyphenyl)-oxalamide and DMA = *N,N*-dimethylacetamide.[12] This MOF was found capable of exchanging Ca^{2+} with Cu^{2+} within seconds, a property that enabled us to utilize **Ca-MOF** as a stationary phase in an ion-exchange column for the removal of Cu^{2+} from aqueous media. Interestingly, after the Cu^{2+} sorption the most expensive part of the MOF, *i.e.* the H_6L ligand, was recycled.

Herein, for the first time, we show that a metal–organic material, namely **Ca-MOF**, shows the capability of both removal and voltammetric determination of heavy metal ions in aqueous media. Interestingly, **Ca-MOF** exhibits particularly high Pb^{2+} sorption capacity (~522 mg g^{-1}), which is among the highest reported for MOFs.[3c,5f] Importantly, a column filled with **Ca-MOF** (1% wt) particles dispersed in silica sand (99% wt) can eliminate traces of Pb^{2+} (~100 ppb) from a wastewater simulant solution (containing a large excess of competitive ions). **Ca-MOF** also shows relatively high sorption capacities for Cd^{2+}, Ni^{2+} and Zn^{2+} which are retained exceptionally well even in the presence of several competitive cations. A combination of spectroscopic and X-ray diffraction methods gave us insights into the structural characteristics of M^{2+} (M^{2+} = Pb^{2+}, Cd^{2+}, Ni^{2+}, Zn^{2+})-loaded materials. We have also fabricated a simple ready-to-use electrochemical sensor based on modified graphite paste with **Ca-MOF**, which was successfully utilized for the determination of Pb^{2+}, Cd^{2+}, Cu^{2+} and Zn^{2+} at μg L^{-1} levels in water solutions by ASV. Overall, this work opens a new avenue for the development of materials that will be highly capable of both heavy metal ion remediation and monitoring in aqueous solutions.

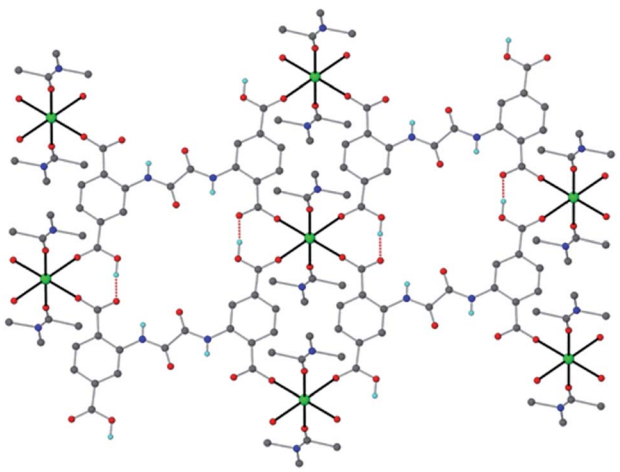

Fig. 1 The structure of **Ca-MOF**. Several H atoms have been removed for clarity. Color code: Ca green, C grey, O red, N blue, and H cyan.

Experimental

Materials

All reagents and solvents were commercially available and used as received.

Synthesis of Ca-MOF

The synthesis of **Ca-MOF** was reported previously by us (it is also provided in the ESI†).[12]

Synthesis of $[Ni(H_4L)(H_2O)_4]\cdot 2DMF$ (1)

An aqueous solution (10 mL) of $Ni(SCN)_2$ (19 mg, 0.06 mmol) was added to a 10 mL DMF solution of H_6L (25 mg, 0.06 mmol) resulting in a non-clear greenish solution. Upon addition of 80 μL of HCl (3 M) no change was observed. The solution was sealed in a glass vial and heated in an isotemp oven at 85 °C for 2 days. Small but well-shaped green needles were formed. The needles were collected by vacuum filtration, washed with DMF (5 mL), and dried in air for 1 h and then in a desiccator over silica gel overnight. Yield: 39.4 mg, 95%. Anal. calcd for $C_{24}H_{32}N_4O_{16}Ni$: C 41.70, H 4.67, N 8.11. Found: C 41.82, H 4.51, N 8.22. IR (KBr pellets, cm^{-1}): 3462 brm, 3328 w, 3216 w, 3075 w, 2930 w, 2813 w, 2492 brw, 1935 brm, 1703 m, 1679 w, 1656 shw, 1627 m, 1579 w, 1575 w, 1511 s, 1446 m, 1418 w, 1371 s, 1307 sh, 1292 m, 1263 m, 1225 w, 1173 s, 1149 w, 1135 w, 1110 s, 1078 m, 1068 sh, 1028 w, 1005 w, 949 m, 915 m, 899 shw, 859 s, 813 m, 800 s, 765 s, 753 w, 678 s, 570 w, 545 w, 511 m, 503 sh, 406 w.

Synthesis of $[Pb_2(H_2L)]\cdot 2H_2O$ (2)

An aqueous solution (10 mL) of $PbCl_2$ (22 mg, 0.06 mmol) was added to a DMF solution (10 mL) of H_6L (25 mg, 0.06 mmol) affording a white non-clear solution. The non-clear solution was then sealed in a glass vial and heated in an isotemp oven at 100 °C for 2 days leading to the formation of colorless plate like single crystals. The single crystals were collected *via* vacuum filtration, washed with DMF (5 mL) and dried in air for 1 h and then in a desiccator over silica gel overnight. Yield: 15.5 mg, 60%. Anal. calcd for $C_{18}H_{12}N_2O_{12}Pb_2$: C 25.06, H 1.40, N 3.25. Found: C 25.17, H 1.31, N 3.33. IR (KBr pellets, cm^{-1}): 3565 w, 3345 br, 3071 br, 1690 m, 1677 sh, 1616 w, 1593 w, 1540 sbr, 1506 s, 1449 s, 1396 w, 1366 s, 1345 sh, 1303 w, 1293 m, 1268 w, 1216 w, 1172 m, 1145 sh, 1080 w, 957 w, 923 w, 912 w, 868 w, 826 w, 813 w, 767 m, 696 w, 686 w, 570 m, 520 m, 486 m.

Physical measurements

Microanalyses (C, H, and N) were performed with an EA 1108 Carlo Erba analyser. IR spectra were recorded on a Shimadzu FT/IR IRAffinity-1 spectrometer with samples prepared as KBr pellets. ^{1}H-NMR spectra were recorded on a Bruker Avance 400 spectrometer operating at 400.13 MHz (^{1}H). Samples were run in a 5 mm probe with DMSO-d_6 as the internal lock and reference. Thermogravimetric analyses (TGA) were performed on a Mettler-Toledo TGA/DSC1 instrument under a N_2 flow of 50 mL min^{-1} from room temperature to 800 °C with a heating rate

of 10 °C min^{-1}. PXRD diffraction patterns were recorded on a Bruker D8 Advance X-ray diffractometer (CuKα radiation, λ = 1.5418 Å). Energy dispersive spectroscopy (EDS) analyses were performed on a JEOL JSM-6390LV scanning electron microscope (SEM) equipped with an Oxford INCA PentaFET-x3 energy dispersive X-ray spectroscopy (EDS) detector. Data acquisition was performed with an accelerating voltage of 20 kV and 120 s accumulation time.

Single crystal X-ray crystallography

The data for the single crystals of **1** and **2** were collected on an Oxford-Diffraction Supernova diffractometer, equipped with a CCD area detector utilizing Cu Kα (λ = 1.5418 Å) radiation. Suitable crystals were mounted on a Hampton cryoloop with Paratone-N oil and transferred to a goniostat where they were cooled for data collection. Empirical absorption corrections (multiscan based on symmetry-related measurements) were applied using CrysAlis RED software. The structures were solved by direct methods using SHELXS-97 and refined by full-matrix least-squares techniques on F^2 with SHELXL-2016/4 (**1**) or SHELXL-2018/3 (ref. 13) (**2**) contained in the WinGX v2014.1 program package.[14] The non-H atoms were treated anisotropically, whereas the methyl, aromatic H and NH hydrogen atoms were placed in calculated, ideal positions and refined as riding on their respective carbon or nitrogen atoms, and the rest of the H atoms were found in the difference map and refined isotropically. Complete crystal data and parameters for data collection and processing are reported in Table S1.† Selected interatomic distances and angles are given in the ESI (Table S2†).

Pair distribution function (PDF) analysis

Samples were measured at 11-ID-C, Advanced Photon sources using X-rays with a wavelength of 0.1174 Å. Scettere 4d intensities were recorded with a 2D detector up to a wave vector of q = 25 A^{-1}. The experimental diffraction patterns were converted to atomic pair distribution functions (PDFs).

ASV procedure

The electrochemical measurements were conducted with a portable electrochemical potentiostat PGSTAT101 (Metrohm Autolab) connected to a laptop. Control and data manipulation (such as baseline correction of the voltammograms) were performed with NOVA 1.8 (Metrohm Autolab) software. Measurements were carried out in a 10 mL glass voltammetric cell equipped with a saturated calomel reference and a Pt wire auxiliary electrode. The square wave anodic stripping voltammetric (SWASV) determination of Pb^{2+}, Cd^{2+} and Cu^{2+} was carried out in 0.10 mol L^{-1} acetate buffer (pH 4.5), while the SWASV analysis of Zn^{2+} was conducted in 1.0 × 10^{-3} mol L^{-1} KCl. The modified working electrode (WE) with **Ca-MOF** was immersed into the test solution and the preconcentration was carried out, for 240 s under stirring at −1.40 V in the case of Cd^{2+} and Cu^{2+} and at −1.60 V for Zn^{2+}. After the accumulation of target metal ions on the WE surface, a SW voltammetric scan (frequency, 50 Hz; pulse height, 40 mV; step increment, 4 mV) was applied to the modified WE to oxidize the target metals and the voltammograms were recorded. Then, the WE was cleaned for traces of remaining accumulated metals for 20 s at 0.20 V.

Preparation of the modified WE with Ca-MOF

The graphite paste electrode (GPE) was prepared by mixing 0.5 g graphite powder (grade #38, Fisher Scientific), 100 mg MOF and 0.20 g paraffin (Merck) in a mortar. The mixture was packed in a plastic syringe (internal radius: 2.4 mm). The electric contact was established by a copper wire passing through the paste. The surface of the WE was polished on a clean filter paper until a smooth surface was obtained. This simple fabrication procedure leads to the production of a ready-to-use-sensor, whose surface can be renewed *via* a slight pressure on the syringe plunger (Fig. S1†). Besides, modified WEs containing 25 and 50 mg **Ca-MOF** in 0.5 g graphite powder and a bare GPE were prepared. The modified WE with 100 mg MOF provided the highest sensitivity for all cations and was finally selected.

Preparation of the column

50 mg of **Ca-MOF** and 5 g of sand (50–70 mesh SiO_2) were mixed using a mortar and pestle and filled in a glass column (0.7 cm ID column).

Batch ion-exchange studies

A typical ion-exchange experiment of **Ca-MOF** with M^{2+} (M^{2+} = Pb^{2+}, Cd^{2+}, Ni^{2+}, Zn^{2+}) is as follows: in a solution of M^{2+} (0.36 mmol) in water (10 mL, pH was not adjusted), the compound **Ca-MOF** (50 mg, 0.06 mmol) was added as a solid. The mixture was kept under sonication and magnetic stirring for 1 h. Then, the solids were isolated by filtration, washed several times with water (5 × 10 mL) and acetone (1 × 5 mL) and dried in a desiccator over silica gel overnight. Yields: **Ni-MOF**: 33 mg, **Zn-MOF**: 28 mg, **Cd-MOF**: 30 mg, and **Pb-MOF**: 36 mg. IR (KBr pellets, cm^{-1}): **Ni-MOF**: 3446 br, 2630 w, 2523 w, 1951 w, 1718 s, 1684 sh, 1627 s, 1599 sh, 1577 s, 1517 s, 1450 s, 1424 w, 1373 m, 1298 s, 1267 w, 1220 w, 1167 m, 1131 w, 1077 w, 948 w, 910 w, 862 m, 796 w, 759 s, 689 w, 569 w, 509 m. **Zn-MOF**: 3521 br, 2627 w, 2516 w, 1717 m, 1683 w, 1627 m, 1603 w, 1576 m, 1517 s, 1451 s, 1424 w, 1374 m, 1298 s, 1267 w, 1220 w, 1166 m, 1133 w, 1076 w, 948 w, 910 w, 862 m, 792 sh, 761 s, 691 w, 568 w, 510 m. **Cd-MOF**: 3501 br, 3071 br, 2496 br, 1683 s, 1630 w, 1601 w, 1573 s, 1517 s, 1450 s, 1424 w, 1366 w, 1294 m, 1263 w, 1220 w, 1165 w, 1129 w, 1070 w, 951 w, 906 w, 863 m, 789 w, 761 s, 688 w, 596 w, 567 m, 504 sh, 487 m. **Pb-MOF**: 3566 w, 3462 br, 3059 brw, 1955 w, 1689 m, 1658 sh, 1625 w, 1556 s, 1530 sh, 1507 s, 1448 s, 1410 w, 1391 w, 1361 brs, 1298 m, 1268 w, 1220 w, 1171 w, 1127 w, 1076 w, 951 w, 898 w, 864 m, 813 w, 803 w, 770 s, 688 m, 599 w, 569 m, 505 m, 483 s. EDS analysis of **M-MOF** (M^{2+} = Ni^{2+}, Zn^{2+}, Cd^{2+} and Pb^{2+}) showed a M : Ca weight or atomic % ratio of ∼100/0% with only traces of Ca detected in the case of **Zn-MOF** (Fig. S2†).

The Pb^{2+} uptake from solutions of various concentrations (1–800 ppm, pH was not adjusted) was studied by the batch method at V : m ∼ 1000 mL g^{-1}, room temperature and 10 min contact. These data were used for the determination of Pb^{2+}

sorption isotherms. Variable pH ion exchange experiments and those with drinking water samples were also carried out with the batch method at $V:m$ ratio ~1000 mL g^{-1}, room temperature and 10 min contact. For the determination of the sorption kinetics, Pb^{2+} ion-exchange experiments of various reaction times (1–60 min) have been performed. For each experiment, a 10 mL sample of Pb^{2+} solution (initial Pb^{2+} concentration = 1 ppm, pH = 7 ± 0.02) was added to each vial (containing 10 mg of **Ca-MOF**) and the mixtures were kept under magnetic stirring for the designated reaction times. The suspensions from the various reactions were filtered and the resulting solutions were analyzed for their Pb content with anodic stripping voltammetry, using a Trace Metal Analyzer (797 VA Computrace, Metrohm AG Ltd, Switzerland). More specifically, a three electrode system was used comprising a Hanging Mercury Drop Electrode (HMDE) as the working electrode, platinum (Pt) as the auxiliary electrode and Ag/AgCl/KCl (3 mol L^{-1}) as the reference electrode. The analysis has been done following the AN-V-086 protocol developed by Metrohm (http://www.metrohm.com/en/applications/#). The same procedure was followed for the removal of Cd^{2+}, Ni^{2+} and Zn^{2+} from aqueous solutions. Each sorption experiment has been done at least twice and the reported sorption data represent the average of sorption results from the different sorption experiments. The difference between the concentrations of metal ions determined from the different sorption experiments was <2%.

Column sorption studies

These studies were performed with a wastewater simulant solution having the following composition: 3 mM $NaHCO_3$, 0.143 mM $NaNO_3$, 10^{-3} mM $NaH_2PO_4 \cdot H_2O$, 5×10^{-2} mM NaF, 0.33 mM $NaSiO_3 \cdot 5H_2O$, 0.99 mM $CaCl_2 \cdot 2H_2O$, 5 mM $MgSO_4 \cdot 7H_2O$, and 4.8×10^{-4} mM Pb^{2+}.[15] The pH of this solution was adjusted to 7. Several bed volumes of the solution were passed through the column and collected at the bottom in glass vials. The solutions were analysed with anodic stripping voltammetry.

Ligand recycling studies

Ni-MOF (30 mg) were immersed in 5 mL HCl 6 M and the resulting white greenish slurry solution was left under stirring for 30 min. The resulting precipitate was centrifuged twice with the addition of H_2O, filtered, washed extensively with H_2O (5 × 5 mL) and dried in a desiccator over silica gel for 2 days. Yield: 17 mg, 72%. **Zn-MOF** (28 mg) was immersed in 5 mL HCl 6 M and the resulting white slurry solution was left under stirring for 30 min. The resulting precipitate was centrifuged twice with the addition of H_2O, filtered, washed extensively with H_2O (5 × 5 mL) and dried in a desiccator over silica gel for 2 days. Yield: 16 mg, 62%. **Cd-MOF** (30 mg) was immersed in 5 mL HCl 6 M and the resulting white greenish slurry solution was left under stirring for 30 min. The resulting precipitate was centrifuged twice with the addition of H_2O, filtered, washed extensively with H_2O (5 × 5 mL) and dried in a desiccator over silica gel for 2 days. Yield: 19 mg, 73%. **Pb-MOF** (36 mg) was immersed in 5 mL HCl 6 M and the resulting white greenish slurry solution was left under stirring for 30 min. The resulting precipitate was centrifuged twice with the addition of H_2O, filtered, washed extensively with H_2O (5 × 5 mL) and dried in a desiccator over silica gel for 2 days. Yield: 13 mg, 50%. The purity of the recycled ligands was confirmed by ^{1}H-NMR (Fig. S3†).

Similarly, recycling of the ligand can be performed for **Pb-MOF** in the ion-exchange column, as reported in our previous publication.[12]

Results and discussion

M^{2+} exchange studies of Ca-MOF

Our previous studies indicated that **Ca-MOF** is a very efficient sorbent for Cu^{2+},[12] whereas this MOF shows very slow exchange for lanthanide ions.[16] In the present study, we investigated the exchange properties of **Ca-MOF** for other divalent metal ions such as Ni^{2+}, Zn^{2+}, Cd^{2+} and Pb^{2+}. The removal of Pb^{2+} and Cd^{2+} from water is of great interest due to the toxicity of these metal ions,[17] whereas selective Ni^{2+} and Zn^{2+} capture is attractive as a recycling process for these metal ions existing in several types of waste (*e.g.* spent batteries and mine wastewater).[18,19] In the following we provide detailed batch M^{2+} (Ni^{2+}, Zn^{2+}, Cd^{2+}, and Pb^{2+}) exchange studies as well as column Pb^{2+} sorption data.

Batch sorption kinetics

At a first step of the Pb^{2+} sorption investigations, the sorption kinetics of the Pb^{2+} of **Ca-MOF** was determined through variable time sorption experiments. Fig. S4A† shows the variation of sorbed Pb^{2+} on **Ca-MOF** as a function of reaction time, with the initial Pb^{2+} concentration being 1 ppm. The kinetic investigations indicated that the capture of Pb^{2+} by **Ca-MOF** was remarkably fast. Interestingly, ~95.6% of the initial Pb^{2+} content was removed within only 1 min of **Ca-MOF**/solution contact, while the time required to reach the sorption equilibrium for Pb was only 5 min. The kinetic data can be fitted very well with Ho and Mckay's pseudo-second-order equation shown below:

$$q_t = \frac{k_2 q_e^2 t}{1 + k_2 q_e t}$$

where q_t = the amount (mg g^{-1}) of the ion sorbed by **Ca-MOF** at different reaction times (t), q_e = the amount (mg g^{-1}) of the metal ion sorbed in equilibrium, and k_2 is the second-order rate constant [g(mg min)$^{-1}$].[20]

Likewise, the sorption of Ni^{2+} by **Ca-MOF** is quite fast, as revealed by the kinetic studies (Fig. S4B†). Specifically, the Ni^{2+} exchange equilibrium is achieved within 5 min. The best fitting of the kinetic data was achieved also with the Ho and Mckay's pseudo-second-order equation. The second order rate constants k_2 for **Ca-MOF** were calculated to be 53.7 ± 5.2 and 6.13 ± 0.82 g(mg min)$^{-1}$, for Pb^{2+} and Ni^{2+} sorption respectively, which indicate that Pb^{2+} exchange was completed significantly faster than the Ni^{2+} sorption process.

Furthermore, the kinetics of Cd^{2+} and Zn^{2+} sorption by **Ca-MOF** was also investigated. The results indicated that the capture of Cd^{2+} by **Ca-MOF** was remarkably fast, as the equilibrium was reached within only 2 min of solution/MOF contact,

with 96.5% of the initial Cd^{2+} amount (C_0 = 1 ppm, pH = 7 ± 0.02) removed from the solution (Fig. S4C†). In the case of Zn^{2+} the ion exchange almost reached its equilibrium after 3 min with ~88.2% removal capacity (Fig. S4D†). The kinetic data for Cd^{2+} and Zn^{2+} sorption can be very well fitted with Lagergren's first-order equation shown below:

$$q_t = q_e[1 - \exp(-K_L t)]$$

where q_e = the amount (mg g^{-1}) of the metal ion sorbed in equilibrium and K_L = the Lagergren or first-order rate constant.[20] The Lagergren constants K_L for **Ca-MOF** were calculated to be 4.01 ± 0.02 and 3.76 ± 0.06 min^{-1}, for Cd^{2+} and Zn^{2+} sorption respectively, revealing the faster sorption process of Cd^{2+} than that of Zn^{2+} by **Ca-MOF**.[20]

Effect of pH

Although the ion exchange studies for **Ca-MOF** were mainly performed at pH = 7 ± 0.02, the MOF material is capable of sorbing metal ions from solutions of a relatively wide pH range (2–8) (Fig. 2).

Specifically, the removal capacities at pH = 3–8 (±0.02) were calculated to be ~98.5, ~97, ~90 and ~97.5% for Pb^{2+}, Cd^{2+}, Zn^{2+} and Ni^{2+} (initial cation concentration = 1 ppm), respectively, whereas **Ca-MOF** retains high removal capability for Pb^{2+} and Cd^{2+} even under highly acidic conditions (~70 and 63% removal capacities at pH = 2, respectively).

Sorption thermodynamics

In order to better understand the equilibrium analysis of the sorption process, Langmuir, Freundlich and Langmuir–Freundlich isotherms were used to fit the sorption equilibrium data. The expressions of the three model equations are as follows:[21]

$$\text{(a) Langmuir } q = q_m \frac{bC_e}{1 + bC_e}$$

$$\text{(b) Freundlich } q = K_F C_e^{\frac{1}{n}}$$

$$\text{(c) Langmuir} - \text{Freundlich } q = q_m \frac{(bC_e)^n}{1 + (bC_e)^n}$$

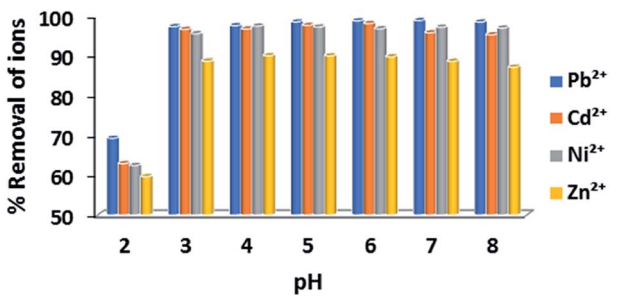

Fig. 2 Percentage (%) sorption of Pb^{2+}, Ni^{2+}, Cd^{2+} and Zn^{2+} cations by **Ca-MOF** in the pH range of 2–8 (initial concentration of each metal ion = 1 ppm).

where q (mg g^{-1}) is the amount of the cation sorbed at the equilibrium concentration C_e (ppm), q_m is the maximum sorption capacity of the sorbent, b (L mg^{-1}) is the Langmuir constant related to the free energy of the sorption, and K_F and $1/n$ are the Freundlich constants. The parameters of Langmuir, Freundlich and Langmuir–Freundlich isotherms, found after the fitting of the isotherm cation sorption data (Fig. 3), are presented in Table 1.

The best fitting of the isotherm data of Pb^{2+}, Ni^{2+} and Zn^{2+} by **Ca-MOF** was achieved by using the Langmuir–Freundlich equation, which is a combination of the Langmuir and Freundlich isotherms.[22] The isotherm data of Cd^{2+} sorption by **Ca-MOF** was fitted by using the Langmuir equation. The maximum sorption capacities were estimated to be 522 ± 26 mg Pb^{2+}, 84 ± 3 mg Ni^{2+}, 220 ± 12 mg Cd^{2+} and 81 ± 5 mg Zn^{2+} per g of **Ca-MOF**. A comparison of the sorption capacities of **Ca-MOF** with those of other heavy metal ion sorbents is provided below. The experimental Ni^{2+} and Zn^{2+} sorption capacities are close to those calculated for the exchange of one Ca^{2+} with one Ni^{2+} or Zn^{2+} (calculated q_m for Ni^{2+} and Zn^{2+} exchange is 73 and 81 mg g^{-1} respectively). However, the Pb^{2+} exchange capacity determined from the isotherm sorption data was found to be two times higher than that calculated for the exchange of one Ca^{2+} with one Pb^{2+} (calculated value = 258 mg g^{-1}). In addition, the experimentally found Cd^{2+} exchange capacity corresponds to the insertion of 1.5 Cd^{2+} per formula unit of the MOF. An explanation about these results is provided in a following section, where the mechanism of the metal ion sorption by **Ca-MOF** is discussed on the basis of various spectroscopic and X-ray diffraction data.

The affinity of **Ca-MOF** for the above cations can be expressed in terms of the distribution coefficient K_d which is given by the following equation:

$$K_d = \frac{V[(C_0 - C_f)/C_f]}{m}$$

where C_0 and C_f are the initial and the equilibrium concentration of the cation (ppm), respectively, V is the volume (mL) of the testing solution and m is the amount of the ion exchanger (g) used in the experiment.[21] The maximum K_d^{Pb} values for **Ca-MOF**, obtained from the batch equilibrium studies, are in the range of 1.5 × 10^3–1.5 × 10^4 mL g^{-1}, which are considered excellent and indicate the exceptional affinity of the material for Pb^{2+} (Fig. S5†).[21] Similarly high K_d values (up to 3.5 × 10^4 mL g^{-1}) were observed for Cd^{2+} exchange, whereas the K_d^{Ni} and K_d^{Zn} values were somewhat smaller (up to 4.5 × 10^3 and 1.1 × 10^4 mL g^{-1} respectively) (Fig. S5†).

Selectivity studies

In order to explore the selectivity of **Ca-MOF** for heavy metal ions *vs.* common competitive cations such as alkali and alkaline earth metal ions, individual sorption experiments for each metal ion were performed in natural spring water (containing 93.1 ppm Ca^{2+}, 1.9 ppm Mg^{2+}, 2.6 ppm Na^+ and 0.7 ppm K^+). The sorption capacities of **Ca-MOF** were calculated to be 98.3%, 98%, 89.4%, 75% and 50% for Pb^{2+}, Cd^{2+}, Ni^{2+}, Cu^{2+} and Zn^{2+},

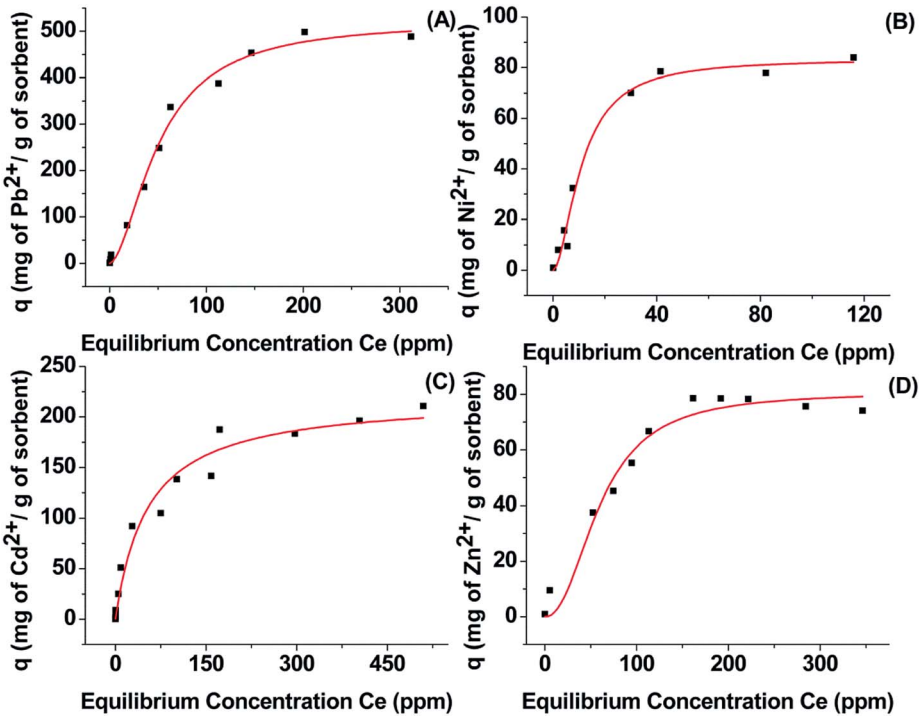

Fig. 3 Isotherm data for Pb^{2+} (A), Ni^{2+} (B), Cd^{2+} (C) and Zn^{2+} (D) sorption by **Ca-MOF**. The red lines represent the fitting of the data with the appropriate model (see the text for details). The model that best describes the sorption of the various metal ions by **Ca-MOF** was decided on the basis of optimum R^2 values and the consistency between experimental and predicted (from the models) q_{max} values.

respectively (Table 2). As a matter of fact, the sorption capacity of **Ca-MOF** seems not to be influenced significantly in the presence of the competitive cations, with the exception of Zn^{2+}, making it an excellent sorbent and also promising for the remediation of real-world wastewater.

As a next step of the selectivity studies, we decided to investigate the selectivity of **Ca-MOF** towards specific heavy metal ions (Table 2). Thus, an aqueous solution containing 1 ppm each of Pb^{2+}, Ni^{2+}, Cd^{2+}, Zn^{2+} and Cu^{2+} was treated with **Ca-MOF**. **Ca-MOF** showed excellent Pb^{2+} and Cd^{2+} removal capacities (~98%), whereas the sorption capacities for Cu^{2+}, Ni^{2+} and Zn^{2+} were found to be moderate (63%, 55% and 40% respectively). This result indicates a significant selectivity of **Ca-MOF** for Pb^{2+} and Cd^{2+} in comparison to the other heavy metal ions. Further selectivity studies were conducted in natural spring water intentionally contaminated with a mixture of the aforementioned cations (Table 2). The removal capacities for Pb^{2+}, Cd^{2+}, and Cu^{2+} were found similar (97%, 97%, and 63% respectively) to those in the experiments involving distilled water. Unexpectedly, the Ni^{2+} removal capacity (~75%) was found somewhat higher compared to that determined in the experiments with distilled water and in addition, no Zn^{2+} sorption capacity was observed. Overall, the selectivity investigations indicated **Ca-MOF** as a highly efficient sorbent for Pb^{2+} and Cd^{2+}, whereas it shows moderate selectivity for Ni^{2+} and Cu^{2+} and relatively low selectivity for Zn^{2+}.

Recycling studies

As also reported in our previous publication,[12] **Ca-MOF** cannot be regenerated after the sorption of the various metal ions. However, after the ion exchange process it is possible to recover the most expensive part of the sorbent, *i.e.* the organic ligand. This recycling process involves treatment of the metal ion-loaded MOF with acidic solution, which results in the decomposition of the MOF through dissolution of the metal ion and protonation of the H_4L^{2-} ligand. The resulted H_6L compound is

Table 1 The parameters of Langmuir, Freundlich and Sips isotherms, found after the fitting of the isotherm sorption data shown in Fig. 3

Metal ion	Langmuir			Freundlich			Langmuir–Freundlich			
	q_m (mg g^{-1})	b (L mg^{-1})	R^2	K_F	n	R^2	q_m (mg g^{-1})	b (L mg^{-1})	n	R^2
Pb^{2+}	667 ± 51	0.012 ± 0.002	0.98	40 ± 14	2.2 ± 0.3	0.93	522 ± 26	0.019 ± 0.002	1.7 ± 0.2	0.99
Ni^{2+}	98 ± 6	0.067 ± 0.014	0.97	15 ± 6	2.6 ± 0.6	0.85	84 ± 3	0.097 ± 0.009	1.6 ± 0.2	0.99
Cd^{2+}	220 ± 12	0.019 ± 0.004	0.97	24 ± 4	2.8 ± 0.2	0.97	301 ± 62	0.007 ± 0.005	0.6 ± 0.1	0.98
Zn^{2+}	99 ± 8	0.014 ± 0.003	0.96	10 ± 4	2.7 ± 0.5	0.90	81 ± 5	0.016 ± 0.002	2.2 ± 0.7	0.97

Table 2 Results of the ion exchange selectivity studies

Sample	C_0 (ppb)	C_e (ppb)	% Removal
Pb^{2+a}	1000	17	98.3
Cd^{2+a}	1000	20	98.0
Ni^{2+a}	1000	106	89.4
Cu^{2+a}	1000	250	75.0
Zn^{2+a}	1000	500	50.0
Mixture of ions[b]	1000[c]	20 (Pb), 20 (Cd), 450 (Ni), 370 (Cu), 600 (Zn)	98 (Pb), 98 (Cd), 55 (Ni), 63 (Cu), 40 (Zn)
Mixture of ions[a]	1000[c]	30 (Pb), 30 (Cd), 250 (Ni), 370 (Cu), 1000 (Zn)	97 (Pb), 97 (Cd), 75 (Ni), 63 (Cu), 0 (Zn)

[a] Natural spring water with Ca^{2+}: 93.1 ppm, Mg^{2+}: 1.9 ppm, K^+: 0.7 ppm, and Na^+: 2.6 ppm. [b] Distilled water. [c] Initial concentration of each ion.

insoluble under acidic conditions and can be easily isolated in a pure form and high yield (Fig. S3†). Details of the recycling process are given the in the Experimental section. We should also note that during the course of our studies (a period > 2 years), we have used recycled ligand samples to prepare new batches of **Ca-MOF**. Such MOF samples have been used for sorption experiments, showing similar results to those obtained with **Ca-MOF** batches synthesized with freshly prepared ligands.

Column ion exchange study

Batch ion exchange studies revealed remarkably high sorption capacities of **Ca-MOF** towards the examined heavy metals. However, industrial wastewater processes require continuous bed flow ion exchange columns. **Ca-MOF** is isolated in the form of relatively large particle-crystals (size 100–300 μm, see Fig. S6†), thus fulfilling an important criterion for a sorbent to be used as a stationary phase in ion exchange columns.[12] The final step in our investigations was the study of the column Pb^{2+} sorption properties of the **Ca-MOF** material. We chose Pb^{2+} among the other heavy metal ions for these studies because of the highly efficient Pb^{2+} sorption properties of **Ca-MOF** and the urgent need to find suitable sorbents to address the pollution of water resources by Pb^{2+} representing one of the most important environmental issues.

As in previous studies,[12] the stationary phase in the column used for Pb^{2+} sorption consisted of **Ca-MOF** and silica sand (**Ca-MOF** : sand mass ratio = 1 : 100). In order to investigate the capability of this column to sorb Pb^{2+} under realistic conditions, we conducted a column sorption study with a ground water simulant solution (its composition is given in the Experimental section) containing traces of Pb^{2+} (initial Pb^{2+} concentration ~ 100 ppb). Note that this solution contained a series of competitive cations with concentrations up to 10^4 times higher than that of Pb^{2+}. The results indicated that ~1.2 L of the solution passed through the column exhibited a concentration <10 ppb. *i.e.* below the allowed USA-EPA and EU levels for Pb^{2+} in water (Fig. 4).

The performance of this column is remarkable considering the fact the stationary phase contained only 50 mg of **Ca-MOF**. Yet, such a small quantity of the MOF was enough to decontaminate a relatively large volume of the wastewater solution, thus demonstrating its potential for real environmental remediation applications. Of course, regeneration/reuse of the **Ca-MOF**/sand column is not possible after its use. However, recycling of the most expensive part of the sorbent, *i.e.* the H_6L ligand, can be performed *via* treatment of the column with a basic solution to decompose the MOF and dissolve the H_4L^{2-} ligand followed by acidification of the solution so that the precipitation of the H_6L ligand is achieved.

Comparison of Ca-MOF with other heavy metal ion MOF sorbents

At this point, we may compare the performance of **Ca-MOF** as a heavy metal ion sorbent with that of other MOF sorbent materials. In Table S3,† the important sorption properties of various MOFs tested so far for the capture of heavy metal ions are shown. It can be seen that only a few MOFs display higher Pb^{2+} sorption capacity than **Ca-MOF**.[5f,g,h] In addition, **Ca-MOF** shows very similar Cd^{2+} sorption capacity to **FJI-H9 MOF** (225 *vs.* 220 mg g^{-1} for **Ca-MOF**), which represents the most effective Cd^{2+} MOF sorbent reported prior to our work.[23] Furthermore, **Ca-MOF** is the only MOF sorbent investigated so far in detail for the sorption of Ni^{2+} and Zn^{2+}. In addition, we should note that **Ca-MOF** is the only MOF tested so far for the removal of Pb^{2+} under flow conditions (*i.e.* using in an ion exchange column of

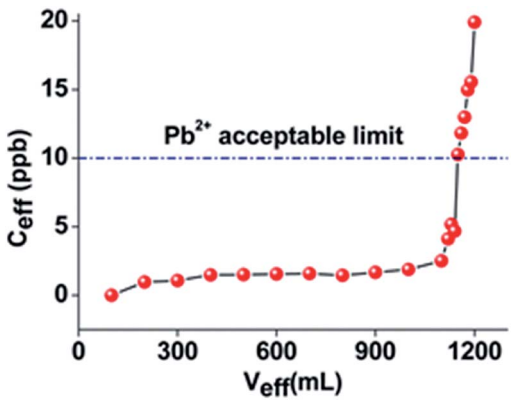

Fig. 4 Column sorption data with a wastewater simulant solution (flow rate ~1.0 mL min^{-1}, one bed volume = 3.5 mL, and stationary phase MOF/sand = 0.05 g : 5 g). The initial concentration of Pb^{2+} was 100 ppb (the concentrations of the other ions are given in the Experimental section). V_{eff} and C_{eff} are the volume (mL) and Pb^{2+} concentration (ppb) of the solution passed through the column (*i.e.* effluent) respectively.

Ca-MOF), *i.e.* under conditions simulating the practical wastewater treatment.

Finally, it is worth comparing the sorption properties of **Ca-MOF** with those of other state-of-the-art heavy metal ion sorbents (besides MOFs), including various sulfur-functionalized materials (clays, LDHs, and mesoporous silica),[24–27] commercial ion exchange resins[28] and metal sulfide ion exchangers (MSIEs).[29] From this comparison (Table S4†), it is apparent that the Pb^{2+} sorption efficiency of **Ca-MOF** exceeds that of other types of sorbents. In addition, the Cd^{2+}, Ni^{2+} and Zn^{2+} uptake capacities of **Ca-MOF** compare well with those of the leading heavy metal ion sorbents.[26,29–31] It is also important to note that **Ca-MOF** shows not only exceptional maximum sorption capacities but also remarkably fast sorption kinetics and high selectivity for heavy metal ions (especially for Pb^{2+} and Cd^{2+}), which surpass those of most known sorbents (Tables S3 and S4†).

Characterization of M^{2+}-loaded MOFs – mechanism of ion exchange

In order to characterize the M^{2+}-loaded MOF materials and gain insight into the possible mechanism of the M^{2+} exchange process, a number of spectroscopic and X-ray diffraction methods were employed. The results obtained are discussed below.

i. Spectroscopic and thermal analyses data. The Energy Dispersive Spectroscopy (EDS) analyses of the M^{2+} (Pb^{2+}, Cd^{2+}, Ni^{2+}, and Zn^{2+})-exchanged **Ca-MOF** indicated complete displacement of the Ca^{2+} by the M^{2+} ions (Fig. S2†). The PXRDs, however, of **M-MOFs** (Fig. S7†) were not informative, revealing a low degree of crystallinity for these materials as a result of the particularly fast ion exchange process. In order to gain some insights into the nature of the exchanged materials we compared their IR spectra (Fig. S8†) and TGA graphs (Fig. S9†). All IR spectra of **M-MOFs** are missing the characteristic DMA bands and look similar but with noticeable differences. Indeed, none of the IR spectra of **M-MOFs** matches perfectly with the IR spectrum of **Cu-MOF**[12] or that of $[Ca(H_4L)(H_2O)_2]\cdot 3H_2O$[12] (the latter two spectra are almost identical). Interestingly, the IR spectra of **Ni-MOF** and **Zn-MOF** are identical, while the IR spectra of **Cd-MOF** and **Pb-MOF** are similar but not identical to each other and they differ from that of **Ni-MOF** and **Zn-MOF**. The TGA graphs of **M-MOFs** show that all metal ion-exchange materials contain various amounts of H_2O (weight losses at temperatures below 150 °C), while they are stable up to ~320 °C. After that temperature, they decompose, with **Ni-MOF** and **Zn-MOF** exhibiting similar decomposition profiles and residues at 800 °C. The TGA graphs of **Cd-MOF** and **Pb-MOF** are quite different from each other and from that of **Ni-MOF** and **Zn-MOF**. Interestingly, the TGA graphs of **M-MOFs** are different from that of **Cu-MOF**. Both IR and TGA indicate that **Ni-MOF** and **Zn-MOF** are quite similar and different from **Cu-MOF**, **Cd-MOF** and **Pb-MOF** with the latter three being different from each other, too.

ii. Synthesis and characterization of $[Ni(H_4L)(H_2O)_4]\cdot 2DMF$ (1) and $[Pb_2(H_2L)]\cdot 2H_2O$ (2). From the above, it is clear that direct information on the nature of **M-MOFs** was quite difficult to obtain. Thus, we aimed at synthesizing new frameworks by reacting several divalent metal ions (*i.e.* $M^{2+} = Pb^{2+}$, Cd^{2+}, Ni^{2+}, Zn^{2+}, Cu^{2+}) with the oxalamide ligand, H_6L, in order to obtain indirect information about the materials that resulted after the ion-exchange procedure of **Ca-MOF**. To this end, we managed to isolate crystalline materials with Ni^{2+} and Pb^{2+}. Interestingly the Ni^{2+}/oxalamide ligand di-anion (H_4L^{2-}) ratio in complex **1** was found to be 1 : 1 while the Pb^{2+}/oxalamide ligand tetra-anion (H_2L^{4-}) ratio in complex **2** was found to be 2 : 1. Both these results were in accordance with the data obtained from the sorption experiments discussed above, where we found that **Ca-MOF** exchanges its one Ca^{2+} per formula unit (the Ca^{2+}/H_4L^{2-} ratio in **Ca-MOF** is 1 : 1) with either one Ni^{2+} or two Pb^{2+} ions.

The reaction of $Ni(SCN)_2$ with H_6L in H_2O/DMF under solvothermal conditions yielded green needles of **1**. Complex **1** crystallizes in the monoclinic space group C_2/c and the unit cell contains one half of Ni^{2+}, one half of H_4L^{2-}, two coordinated H_2O molecules and one solvate DMF molecule. The Ni^{2+} ion resides on an inversion center with 50% site occupancy, adopts an octahedral coordination geometry and is surrounded by six O atoms. The four equatorial O atoms originate from four terminal water molecules while the two apical positions are occupied by two monodentately coordinated carboxylate groups originating from two different ligand moieties (H_4L^{2-}) that adopt the $\eta^1{:}\eta^1{-}\mu_2$ coordination mode leading to a 1D zig-zag chain running parallel to the *b* axis (Fig. 5). The two pending carboxylic groups (one unique) of the H_4L^{2-} ligand form hydrogen bonds with the DMF solvates. There are also several intra- and inter-chain H-bonds involving the terminal H_2O molecules and several O donor atoms of the H_4L^{2-} ligand that increase the dimensionality of the material to 3D. The purity of complex **1** was verified by PXRD (Fig. S10†).

The reaction of $PbCl_2$ with H_6L in H_2O/DMF under solvothermal conditions yielded block colorless crystals of **2**. Complex **2** crystallizes in the orthorhombic space group *Pbcn* and the unit cell contains two Pb^{2+} ions with 50% occupancy, one half of H_2L^{4-} and one solvate H_2O molecule being disordered over two positions with 50% occupancy. Both Pb^{2+} ions

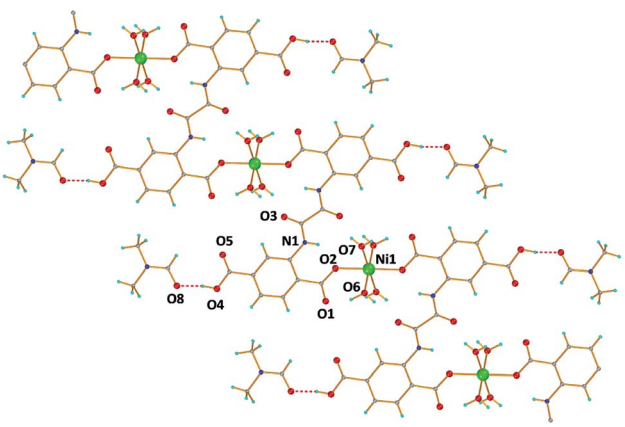

Fig. 5 A labeled plot of $[Ni(H_4L)(H_2O)_4]\cdot 2DMF$ (**1**). Color code: Ni green, C grey, O red, N blue, and H cyan.

reside on the 2-fold rotation axis and both are surrounded by six carboxylate O atoms originating from four different H_2L^{4-} ligands. The coordination environment around each Pb atom is far from octahedral owing to the significant space occupied by the lone electron pair on each Pb^{2+}. Each of the four carboxylate groups of the tetra-anionic oxalamide ligand (H_2L^{4-}) adopts the $\eta^1{:}\eta^2{-}\mu_2$ coordination mode, bridging either two Pb1 or two Pb2 ions. Therefore, each H_2L^{4-} anion serves as a μ_8 bridging ligand creating, along with the Pb^{2+} ions, a double-walled layer laying parallel to the *ac* plane. The one-dimensional channels formed within the double-walled layer are hosting the solvate H_2O molecules (Fig. 6). The purity of complex **2** was verified by PXRD (Fig. S11†). Unfortunately, our efforts to isolate crystalline MOFs of H_6L with Zn^{2+} and Cd^{2+} have not been fruitful, so far.

iii. PDF studies. As mentioned above, the PXRD patterns of the metal ion-loaded MOFs (Fig. S7†) indicated structures with very low crystallinity and thus, the identification of their structural characteristics was a quite difficult task. Therefore, we conducted high-energy XRD experiments coupled to atomic pair distribution function analysis (PDF).

This approach has proven very useful in structure studies of materials with limited structural coherence, ranging from crystals with intrinsic disorder to amorphous solids and liquids.[32] The experimental atomic PDFs (Fig. S12†) show sharp peaks at low-*r* distances reflecting the presence of a well-defined short-range atomic order. The PDFs also show subsequent broad oscillations indicating the presence of a medium-range atomic order. The oscillations are very well-defined with the PDFs for **Ni-MOF**, **Zn-MOF** and **Cu-MOF** in comparison to **Pb-MOF** and **Cd-MOF**. The observation indicates that the former Ni^{2+}, Zn^{2+} and Cu^{2+} loaded MOFs are more ordered locally as compared to the latter (*i.e.* Pd^{2+} and Cd^{2+}-loaded materials). As can also be seen in Fig. S12,† the atomic PDFs for **Ni-MOF**, **Zn-MOF** and **Cu-MOF** are similar indicating that the materials share common structural features. In addition, it can be seen that there are some common features in the PDFs of **Pb-MOF** and **Cd-MOF**. Selected atomic pair distances for **Ni-MOF**, **Zn-MOF**, **Cu-MOF**, **Pb-MOF**, **Cd-MOF** and **Ca-MOF** (computed) are shown in Fig. 7.

The distances for different metal ion-loaded materials are somewhat different reflecting the different compositions and/or sizes of metal ions. Experimental (for **Ni-MOF** and **Pb-MOF**) and computed PDFs derived from crystal structure models of $[Ni(H_4L)(H_2O)_4]\cdot 2DMF$ (**1**) and $[Pb_2(H_2L)]\cdot 2H_2O$ (**2**) are shown in Fig. 8.

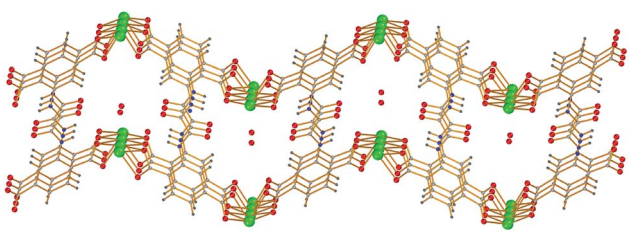

Fig. 6 The one-dimensional channels formed within the double-walled layer of $[Pb_2(H_2L)]\cdot 2H_2O$ (**2**) hosting the solvate H_2O molecules. Color code: Pb green, C grey, O red, N blue, and H cyan.

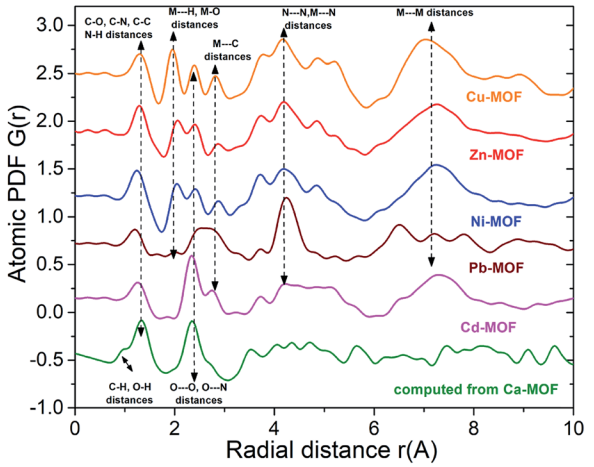

Fig. 7 Low-*r* part of experimental atomic PDFs for **Cu-MOF**, **Zn-MOF**, **Ni-MOF**, **Pb-MOF** and **Cd-MOF**. Selected atomic pair distances are marked with vertical broken lines. Computed PDF for **Ca-MOF** is also shown.

As can be seen in Fig. 8, the local atomic structure of **Ni-MOF** is close to that of the respective crystal structure of **1**. The comparison of the PDF of **Pb-MOF** with that computed from the structure of **2** also revealed several similarities between them. First three PDF peaks for **Pb-MOF** are well-defined and positioned at about 1.2, 2.6 and 4.2 Å. Similarly to the PDF of **Pb-MOF**, the computed PDF of **2** shows peaks at about 1.2 and 4.2 Å. Contrary to the PDF of **Pb-MOF**, the calculated PDF of **2** does not show a well-defined peak but only a spike in the vicinity of 2.4 A. The spike can be attributed to Pb–O distances and it also appears as a second neighbour peak in the computed PDF of **Ca-MOF**. Evidently, the **Pb-MOF** and compound **2** show common structural features.

iv. Mechanism of the ion exchange process. The mechanism of the capture of metal ions by **Ca-MOF** can be better described as an ion exchange-chemical sorption process. Actually, Ca^{2+} is weakly bound to the polycarboxylate ligand (there are mainly

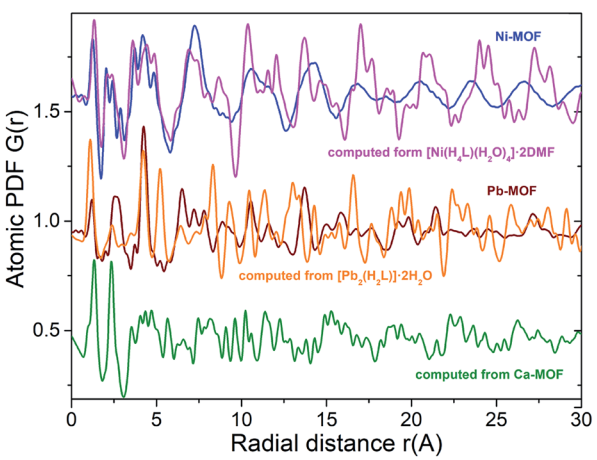

Fig. 8 Comparison between experimental (**Ni-MOF** and **Pb-MOF**) and model (**1** and **2**) PDFs.

electrostatic Ca^{2+}–ligand interactions), whereas the inserted metal ions (Cu^{2+}, Cd^{2+}, Pb^{2+}, Ni^{2+}, and Zn^{2+}) form strong covalent (dative) bonds with the ligands. There is no dissociation of the MOF in water as revealed by ^1H NMR experiments in which the **Ca-MOF** solid was placed in D_2O.[12] The ^1H NMR data showed that no ligand is leached from the MOF.[12] Even in the presence of metal ions (such as Zn^{2+}) in water solution, we could not observe any leaching of the ligand in water. In addition, leaching of the ligand has not been observed from **Ca-MOF** in the pH range of 2–8. From the above spectroscopic and analytical data, the exchange of Ca^{2+} in **Ca-MOF** with Pb^{2+}, Cd^{2+}, Ni^{2+} and Zn^{2+} can be summarized by eqn (1)–(3):

$$[Ca(H_4L)(DMA)_2]\cdot 2DMA + 2Pb^{2+} + xH_2O \rightarrow [Pb_2(H_2L)]\cdot xH_2O + Ca^{2+} + 2H^+ + 4DMA \quad (1)$$

$$[Ca(H_4L)(DMA)_2]\cdot 2DMA + 1.5Cd^{2+} + xH_2O \rightarrow [Cd_{1.5}(H_4L)_{0.5}(H_2L)_{0.5}]\cdot xH_2O + Ca^{2+} + H^+ + 4DMA \quad (2)$$

$$[Ca(H_4L)(DMA)_2]\cdot 2DMA + M^{2+} + (x+4)H_2O \rightarrow [M(H_4L)(H_2O)_4]\cdot xH_2O + Ca^{2+} + 4DMA \ (M^{2+} = Ni^{2+}, Zn^{2+}) \quad (3)$$

Based on the results from spectroscopic, thermal and X-ray diffraction methods, some suggestions for the possible structures of metal ion-loaded MOFs can be provided. Thus, PDF, IR and TGA revealed that **Ni-MOF** and **Zn-MOF** present identical structures which are closely related to the structure of $[Ni(H_4L)(H_2O)_4]\cdot 2DMF$ (**1**) reported in this work. In addition, PDF data indicated that **Pb-MOF** has some common structural features with $[Pb_2(H_2L)]\cdot 2H_2O$ (**2**) also described in this work. These results are consistent with the chemical composition (metal to ligand molar ratio) of **Ni-MOF**, **Zn-MOF** and **Pb-MOF** determined from the sorption data. Finally, PDF and IR data showed that there are some similarities between the structures of **Pb-MOF** and **Cd-MOF**, but they are not identical. This is also in accordance with the sorption data which revealed somewhat different metal to ligand molar ratios for **Pb-MOF** and **Cd-MOF** which are 2 : 1 and 1.5 : 1, respectively.

Determination of Pb^{2+}, Cu^{2+}, Cd^{2+}, and Zn^{2+} by ASV at a modified GPE with Ca-MOF

From the above discussed sorption data and our previous work,[12] it became apparent that **Ca-MOF** is an excellent and selective sorbent for various heavy metal ions. Such a highly efficient sorbent as **Ca-MOF** is suitable to be used in electrodes for preconcentration of heavy metal ions and their determination *via* anodic stripping voltammetry (ASV). We have thus fabricated a stand-alone and ready-to-use MOF-based syringe electrode. The analytical performance of the modified GPE with **Ca-MOF** was investigated by conducting preliminary quantitative ASV analyses at various concentrations (10–60 μg L^{-1}) of Pb^{2+}, Cu^{2+}, Zn^{2+} and Cd^{2+}. These metal cations were selected as model analytes in order to show the performance of the **Ca-MOF**/sensor in a wide range of potentials. Besides, the **Ca-MOF**/sensor was capable of detecting more than one heavy metal ion in a single run, such as Pb^{2+} and Cd^{2+} (Fig. S13†).

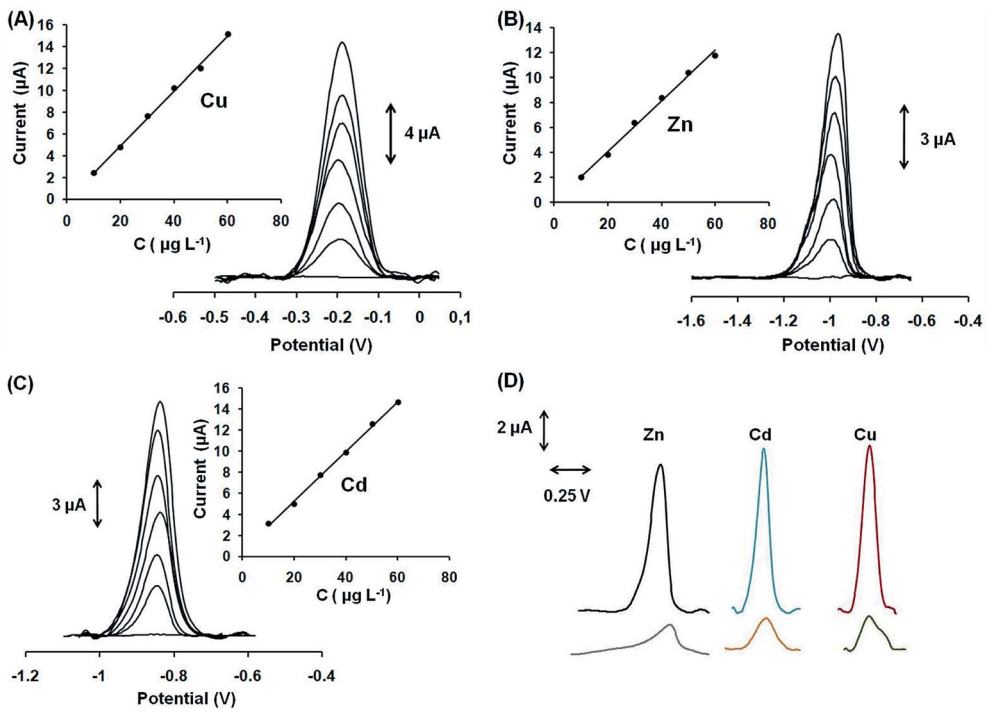

Fig. 9 SWASV voltammograms and respective calibrations plots in the range of 10–60 μg L^{-1} (step 10 μg L^{-1}) of (A) Cu^{2+} in 0.1 mol L^{-1} acetate buffer, (B) Zn^{2+} in 1×10^{-3} mol L^{-1} KCl, and (C) Cd^{2+} in 0.1 mol L^{-1} acetate buffer (pH 4.5). (D) SWASV voltammograms of 30 μg L^{-1} of Zn^{2+}, Cd^{2+}, and Cu^{2+} (black, blue, and red lines respectively) obtained with the modified GPE with **Ca-MOF** and SWASV voltammograms of 30 μg L^{-1} of Zn^{2+}, Cd^{2+}, and Cu^{2+} (gray, orange, and green lines, respectively) obtained with the bare GPE. Other voltammetric parameters are noted in the text.

The sensor exhibited linear concentration dependence in the examined concentration ranges for all metal ions with correlation coefficients (R^2) higher than 0.99 in all cases, as depicted in Fig. 9 (panels A–C) and Fig. S14.† The limits of detection (LODs) (calculated as three times the standard deviation of the y residuals of the calibration points divided by the slope of the calibration plot) were 0.64 μg L^{-1} for Pb^{2+}, 1.4 μg L^{-1} for Cu^{2+}, 1.1 μg L^{-1} for Zn^{2+} and 1.3 μg L^{-1} for Cd^{2+}, which were comparable to, or lower than, those of other electrochemical sensors.[33–35] The within-sensor reproducibility (expressed as the % relative standard deviation (% RSD) of repetitive measurements ($n = 5$) of 30 μg L^{-1} of each cation at the same sensor) was lower than 4.2%, while the between-sensor reproducibility (% RSD at four different sensors) was lower than 5.8% at the 30 μg L^{-1} level. Besides, the shelf-life of the modified GPE with **Ca-MOF** was tested over a period of 2 months and a t-test demonstrated that the ASV response remained statistically stable. These results verify the suitability of the proposed sensor for monitoring selected trace heavy metal ions. Besides, the ASV detection sensitivity of Pb^{2+}, Cu^{2+}, Cd^{2+}, and Zn^{2+} at the modified GPE with **Ca-MOF** was about 5 times higher than that of the unmodified GPE (Fig. 9D), and also better-shaped stripping peaks with a lower background were obtained, indicating the enhanced electrochemical properties of **Ca-MOF**.

Compared to conventional, bismuth- and antimony-film electrodes, which are the most commonly used mercury-free transducers in ASV determination of heavy metals, the presented modified GPE with **Ca-MOF** is also able to determine Cu^{+2}. At bismuth or antimony film electrodes, Cu determination is normally not possible since the oxidation peak of Cu appears outside the useful potential window of these electrodes.[36–38] On the other hand, the existing MOF-based electrodes have shown single metal ion ASV detection properties (as they can determine only one cation), while the modified GPE with **Ca-MOF** presented multi-detection capabilities.[7–10] Only two reports appear in the pertinent literature that use MOF-based electrodes for the ASV detection of four metal ions, but in these applications the MOFs were drop-cast on bare glassy carbon electrodes (GCEs).[11] According to this protocol, each time and before each electrochemical measurement the bare GCE is abraded with appropriate paper, polished with alumina slurries, sonicated in suitable solutions for cleaning and then the MOF is dripped onto the GCE and air-dried. Therefore, these MOF-based electrodes cannot be considered as ready-to-use sensors, since they require a multistep reconstruction before each electrochemical measurement. Last but not least, so far, no MOF-based electrodes have been reported for ASV trace determination of Zn(II).

Conclusions

In conclusion, the MOF $[Ca(H_4L)(DMA)_2]\cdot 2DMA$ (**Ca-MOF**) was shown to be a highly selective and efficient sorbent for heavy metal ions, especially for Pb^{2+} and Cd^{2+} being some of the most dangerous pollutants in various types of wastewater. It is also important that a low cost column based on **Ca-MOF** and silica sand was found particularly effective to decontaminate relatively large quantities of simulated wastewater containing traces of Pb^{2+} (100 ppb) and a series of competitive ions in high concentrations. The latter result indicated that **Ca-MOF** might find practical application in heavy metal ion remediation of polluted water. Pair distribution function (PDF) data provided us insight into the structure of M^{2+}-exchanged materials. Thus, these data revealed close similarities of the structures of the Ni^{2+}, Zn^{2+} and Cu^{2+}-loaded materials with that of the crystalline $[Ni(H_4L)(H_2O)_4]\cdot 2DMF$ (**1**) compound reported in this work. In addition, PDF studies indicated that the Pb^{2+}-loaded material shares common structural features with the $[Pb_2(H_2L)]\cdot 2H_2O$ (**2**) compound also described here. Motivated by the excellent heavy metal ion sorption properties of **Ca-MOF**, we have developed a simple ready-to-use electrochemical sensor based on modified graphite paste with **Ca-MOF**. This sensor was capable of analysing Pb^{2+}, Cu^{2+}, Zn^{2+} and Cd^{2+} *via* anodic stripping voltammetry (ASV) and particularly low detection limits (0.64–1.4 μg L^{-1}) were achieved for these metal ions. Actually, this is the first time that a MOF shows such a dual function, *i.e.* it is suitable for both sorption and electrochemical determination of heavy metal ions. Thus, an avenue is opened for the development of a new family of materials that would be employed in both environmental remediation and monitoring. Research in our groups is currently focused towards this direction.

Conflicts of interest

There are no conflicts to declare.

Acknowledgements

AP would like to thank the State Scholarships foundation (IKY) for a post-doctoral research scholarship, funded by the Action "Supporting Post-Academic Researchers" from the resources of the NF "Human Resources Development, Education and Lifelong Learning" with Priority Axes 6, 8, and 9 and co-funded by the European Social Fund – ESF and the Greek State. This work was partially supported by the Special Account for Research Grants (SARG) of the National and Kapodistrian University of Athens (UoA). The work was also supported in part by DOE grant DE-SC0006877. The Bodossaki Foundation is gratefully acknowledged for donating the TGA to UoA.

Notes and references

1 (*a*) B. Sarkar, *Heavy metals in the environment*, CRC Press, 2002; (*b*) G. M. Naja and B. Volesky, Toxicity and sources of Pb, Cd, Hg, Cr, As, and radionuclides in the environment, in *Heavy Metals in the Environment*, ed. L. K. Wang, J. P. Chen, Y. Hung and N. K. Shammas, CRC Press, 2009; (*c*) L. M. Plum, L. Rink and H. Haase, *Int. J. Environ. Res. Public Health*, 2010, **7**, 1342–1365.

2 A. Diamantis, A. Margariti, A. D. Pournara, G. S. Papaefstathiou, M. J. Manos and T. Lazarides, *Inorg. Chem. Front.*, 2018, **5**, 1493–1511 and references cited therein.

3 (*a*) M. Eddaoudi, D. B. Moler, H. Li, B. Chen, T. M. Reineke, M. O'Keeffe and O. M. Yaghi, *Acc. Chem. Res.*, 2001, **34**, 319–330; (*b*) S. Horike, S. Shimomura and S. Kitagawa, *Nat. Chem.*, 2009, **1**, 695–704; (*c*) P. Kumar, A. Pournara, K. H. Kim, V. Bansai, S. Rapti and M. J. Manos, *Prog. Mater. Sci.*, 2017, **86**, 25–74; (*d*) J. M. Taylor, T. Komatsu, S. Dekura, K. Otsubo, M. Takata and H. Kitagawa, *J. Am. Chem. Soc.*, 2015, **137**, 11498–11506.

4 (*a*) C. K. Brozek and M. Dinca, *Chem. Soc. Rev.*, 2014, **43**, 5456–5467; (*b*) D. T. Genna, A. G. Wong-Foy, A. J. Matzger and M. S. Sanford, *J. Am. Chem. Soc.*, 2013, **135**, 10586–10589; (*c*) J. Yu, Y. Cui, C. Wu, Y. Yang, Z. Wang, M. O'Keeffe, B. Chen and G. Qian, *Angew. Chem., Int. Ed.*, 2012, **51**, 10542–10545; (*d*) Z. Wang, J. H. Zhang, J. J. Jiang, H. P. Wang, Z. W. Wei, X. Zhu, M. Pan and C. Y. Su, *J. Mater. Chem. A*, 2018, **6**, 17698–17705; (*e*) Y. X. Tan, Y. P. He and J. Zhang, *Chem. Commun.*, 2011, **47**, 10647–10649.

5 (*a*) A. V. Desai, B. Manna, A. Karmakar, A. Sahu and S. K. Ghosh, *Angew. Chem., Int. Ed.*, 2016, **55**, 7811–7815; (*b*) L. Carlucci, G. Ciani, S. Maggini, D. M. Proserpio and M. Visconti, *Chem.–Eur. J.*, 2010, **16**, 12328–12341; (*c*) H. R. Fu, Z. X. Xu and J. Zhang, *Chem. Mater.*, 2015, **27**, 205–210; (*d*) H. Fei, C. H. Pham and S. R. J. Oliver, *J. Am. Chem. Soc.*, 2012, **134**, 10729–10732; (*e*) Y. Feng, Y. Bi, W. Zhao and T. Zhang, *J. Mater. Chem. A*, 2016, **4**, 7596–7600; (*f*) J. Li, X. Wang, G. Zhao, C. Chen, Z. Chai, A. Alsaedi, T. Hayat and X. Wang, *Chem. Soc. Rev.*, 2018, **47**, 2322–2356; (*g*) M. Mon, R. Bruno, J. Ferrando-Soria, D. Armentano and E. Pardo, *J. Mater. Chem. A*, 2018, **6**, 4912–4947; (*h*) Q. Gao, J. Xu and X.-H. Bu, *Coord. Chem. Rev.*, 2019, **378**, 17–31; (*i*) S. Rapti, S. A. Diamantis, A. Dafnomili, A. Pournara, E. Skliri, G. S. Armatas, A. C. Tsipis, I. Spanopoulos, C. D. Malliakas, M. G. Kanatzidis, J. C. Plakatouras, F. Noli, T. Lazarides and M. J. Manos, *J. Mater. Chem. A*, 2018, **6**, 20813–20821; (*j*) R. J. Drout, K. Otake, A. J. Howarth, T. Islamoglu, L. Zhu, C. Xiao, S. Wang and O. K. Farha, *Chem. Mater.*, 2018, **30**, 1277–1284.

6 A. Economou and C. Kokkinos, Advances in Stripping Analysis of Metals, in *Electrochemical Strategies in Detection Science*, ed. D. Arrigan and M. Thomson, RSC, 2016.

7 F. Cai, Q. Wang, X. Chen, W. Qiu, F. Zhan, F. Gao and Q. Wang, *Biosens. Bioelectron.*, 2017, **98**, 310–316.

8 M. Roushani, A. Valipour and Z. Saedi, *Sens. Actuators, B*, 2016, **233**, 419–425.

9 H. Guo, Z. Zheng, Y. Zhang, H. Lin and Q. Xu, *Sens. Actuators, B*, 2017, **248**, 430–436.

10 H. Guo, D. Wang, J. Chen, W. Weng, M. Huang and Z. Zheng, *Chem. Eng. J.*, 2016, **289**, 479–485.

11 (*a*) D. Wang, Y. Ke, D. Guo, H. Guo, J. Chen and W. Weng, *Sens. Actuators, B*, 2015, **216**, 504–510; (*b*) M. Lu, Y. Deng, Y. Luo, J. Lv, T. Li, J. Xu, S.-W. Chen and J. Wang, *Anal. Chem.*, 2018, **91**, 888–895.

12 A. Margariti, S. Rapti, A. D. Katsenis, T. Friščić, Y. Georgiou, M. J. Manos and G. S. Papaefstathiou, *Inorg. Chem. Front.*, 2017, **4**, 773–781.

13 G. M. Sheldrick, *Acta Crystallogr., Sect. A: Found Crystallogr.*, 2008, **64**, 112–122.

14 L. J. Farrugia, *J. Appl. Crystallogr.*, 2012, **45**, 849–854.

15 F. Pinakidou, E. Kaprara, M. Katsikini, E. C. Paloura, K. Simeonidis and M. Mitrakas, *Sci. Total Environ.*, 2016, **551–552**, 246–253.

16 A. Margariti, A. D. Pournara, M. J. Manos, T. Lazarides and G. S. Papaefstathiou, *Polyhedron*, 2018, **153**, 24–30.

17 *Handbook on the Toxicology of Metals*, ed. G. F. Nordberg, B. A. Fowler, M. Nordberg and L. T. Friberg, Elsevier, 3rd edn, 2007.

18 V. Coman, B. Robotin and P. Ilea, *Resour., Conserv. Recycl.*, 2013, **73**, 229–238.

19 K. Tanong, J.-F. Blais and G. Mercier, *Recent Pat. Eng.*, 2014, **8**, 13–23.

20 A. Benhammou, A. Yaacoubi, L. Nibou and B. Tanouti, *J. Colloid Interface Sci.*, 2005, **282**, 320–326.

21 (*a*) M. J. Manos and M. G. Kanatzidis, *Chem.–Eur. J.*, 2009, **15**, 4779–4784; (*b*) M. J. Manos, N. Ding and M. G. Kanatzidis, *Proc. Natl. Acad. Sci. U. S. A.*, 2008, **105**, 3696–3699.

22 G. P. Jeppu and T. P. Clement, *J. Contam. Hydrol.*, 2012, **129–130**, 46–53.

23 H. Xue, Q. Chen, F. Jiang, D. Yuan, G. Lv, L. Liang, L. Liu and M. Hong, *Chem. Sci.*, 2016, **7**, 5983–5988.

24 I. L. Lagadic, M. K. Mitchell and B. D. Payne, *Environ. Sci. Technol.*, 2001, **35**, 984–990.

25 L. Ma, Q. Wang, S. M. Islam, Y. Liu, S. Ma and M. G. Kanatzidis, *J. Am. Chem. Soc.*, 2016, **138**, 2858–2866.

26 S. Ma, Q. Chen, H. Li, P. Wang, S. M. Islam, Q. Gu, X. Yang and M. G. Kanatzidis, *J. Mater. Chem. A*, 2014, **2**, 10280–10289.

27 J. S. Lee, S. Gomez-Salazar and L. L. Tavlarides, *React. Funct. Polym.*, 2001, **49**, 159–172.

28 S. Chamarthy, C. W. Seo and W. E. Marshall, *J. Chem. Technol. Biotechnol.*, 2001, **76**, 593–597.

29 M. J. Manos and M. G. Kanatzidis, *Chem. Sci.*, 2016, **7**, 4804–4824.

30 D. Sarma, S. M. Islam, K. S. Subrahmanyam and M. G. Kanatzidis, *J. Mater. Chem. A*, 2016, **4**, 16597–16605.

31 J.-R. Li, L. Xu, M.-L. Fu, Y.-X. Wang and H. Xiao, *Inorg. Chem. Front.*, 2018, **5**, 403–412.

32 (*a*) H. P. Klug and L. E. Alexander, *X-Ray Diffraction Procedures for Polycrystalline and Amorphous Materials*, Wiley, 1974; (*b*) T. Egami and S. Billinge, *Underneath the Bragg Peaks: Structural Analysis of Complex Materials*, Pergamon Press, 2012.

33 L. Xiao, H. Xu, S. Zhou, T. Song, H. Wang, S. Li, W. Gan and Q. Yuan, *Electrochim. Acta*, 2014, **143**, 143–151.

34 N. Serrano, J. M. Díaz-Cruz, C. Ariño and M. Esteban, *Anal. Bioanal. Chem.*, 2009, **396**, 1365–1369.

35 P. S. Adarakatti, V. Gangaiah and A. Siddaramanna, *Mater. Sci. Semicond. Process.*, 2018, **84**, 157–166.

36 A. Economou and P. R. Fielden, *Analyst*, 2003, **128**, 205–213.

37 C. Kokkinos and A. Economou, *Curr. Anal. Chem.*, 2008, **4**, 183–190.

38 N. Serrano, J. M. Díaz-Cruz, C. Ariño and M. Esteban, *TrAC, Trends Anal. Chem.*, 2016, **77**, 203–213.